Colloids and Surfaces A 580 (2019) 123781

Contents lists available at ScienceDirect

Colloids and Surfaces A

journal homepage: www.elsevier.com/locate/colsurfa

Interaction energies for hollow and solid cylinders: Role of aspect ratio and particle orientation

Allan Gomez-Flores[a], Scott A. Bradford[b,*], Lei Wu[c], Hyunjung Kim[a,*]

[a] Department of Mineral Resources and Energy Engineering, Chonbuk National University, 567, Baekje-daero, Deokjin-gu, Jeonju, Jeonbuk 54896, Republic of Korea
[b] US Salinity Laboratory, USDA, ARS, Riverside, CA, USA
[c] Department of Civil Engineering, Ohio University, Athens, OH 45701, USA

GRAPHICAL ABSTRACT

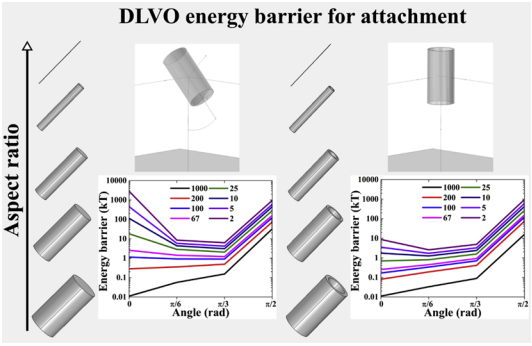

ARTICLE INFO

Keywords:
Cylinder
Hollow
Solid
Aspect ratio
Angle
DLVO
SEI

ABSTRACT

Particles of various shapes (e.g., spheres or rods), sizes (e.g., nm to microns), interiors (e.g., solid or hollow), and materials are used in many industrial and environmental applications. The Derjaguin–Landau–Verwey–Overbeek (DLVO) theory has commonly been used to calculate and predict the adhesive interaction of these particles with solid surfaces. However, DLVO theory treats these particles as equivalent spheres for simplicity ignoring shape in numerous cases. The surface element integration (SEI) approach allows DLVO theory to be extended for different particle shapes, orientations, and interiors. In this study, the SEI approach was applied to calculate the interaction energy between hollow and solid cylinders with a flat surface. The effect of aspect ratio and particle orientation on interaction energies was investigated under different solution chemistry conditions. Our study is relevant for an extensive range of particle aspect ratios, ranging from nanosized particles such as carbon nanotubes or nanowires, which have high aspect ratios, to micron-sized particles such as bacteria, which have low aspect ratios. The energy barrier tended to increase when the angle that the larger axis of the particle made with the normal to the surface changed from perpendicular (0 rad) to parallel ($\pi/2$ rad). The aspect ratio did not affect the trend of the energy barrier for solid (200–1000) and hollow (25–1000) cylinders of relatively high aspect ratios, but it produces a non-monotonic trend for solid (2–100) and hollow (2–10) cylinders of low aspect ratios. The present study advances our understanding of adhesive interactions for particles having a wide range of aspect ratios and interior properties at various orientations with the surface.

* Corresponding authors.
E-mail addresses: Scott.Bradford@ars.usda.gov (S.A. Bradford), kshjkim@jbnu.ac.kr (H. Kim).

https://doi.org/10.1016/j.colsurfa.2019.123781
Received 24 June 2019; Received in revised form 8 August 2019; Accepted 8 August 2019
Available online 09 August 2019
0927-7757/ © 2019 Elsevier B.V. All rights reserved.

1. Introduction

Particles in nature exhibit a myriad of shapes, which can be partially or completely represented by regular or irregular geometric shapes [1]. Such particles include colloids of different sizes, for example micro- or nano-colloids, viruses, organic macromolecules, soil and mineral particles, and bacteria. Different shapes, including spheres, barrels, ellipsoids, cylinders, cubes, and tetrahedral, have been used in environmental and colloid science studies [2–4]. Ellipsoid, cylindrical, rod-like, and bullet-like particles have been the special focus of research because they can be used as surrogates for various bacteria and engineered nanoparticles or because they exhibit high performances in selected applications [5–9]. Ellipsoids and cylinders can have very broad aspect ratios, usually defined as the proportion between the short and long axes. For example, carbon nanotubes (CNTs), either single-walled (SWCNTs) or multi-walled (MWCNTs), are engineered nanoparticles with large aspect ratios that are extensively used in applications such as vaccines, scaffolds, biosensors, antistatic coatings, and bullet-proof vests [10]. The transport and deposition of SWCNTs and MWCNTs have been the center of attention of several studies because of their environmental impact [10–17].

Several studies have considered particle aspect ratios that are smaller [2,3,7,18–34] or larger [11–16,35–37] than 25 to conduct experiments in broad fields of science. Important results from those studies can be summarized as follows. Aspect ratio affects settling of particles. Self-assembly is different according to aspect ratio. Low aspect ratio (≈ 4) particles assemble in a smectic order and high aspect ratio (> 10) particles in a nematic order. Short length cylinders tend to self-assembly on end-to end orders. Fabrication of arrays of nanoparticles can be tuned by water chemistry and order varies according to aspect ratio. An increase in aspect ratio of particle increases particle retention. Uptake of particles in liver increases as aspect ratio decreases. Aspect ratio influences interactions with polymer layers. The interaction with a cell surface and consequent mechanism of particle uptake by a cell varies according to aspect ratio. It can been perceived, therefore, the importance of investigating the influence of aspect ratio.

Deposition of particles is commonly interpreted using the Derjaguin–Landau–Verwey–Overbeek (DLVO) theory [2,4,8,9], which describes the interaction of a particle with a surface as the sum of van der Waals (VDW) attraction and electrostatic double layer (EDL) interaction. Mathematical descriptions of DLVO interactions are normally based on the Derjaguin assumption (DA) that particles are spherical (equivalent sphere) for simplicity in many cases, distance of interaction is shorter than the radii of curvature of the particle, interaction energy between two surfaces occurs at small region around the point of closest approach, and other implications after assumptions [38]. Some studies have discussed the disadvantages of the DA and proposed modifications to DLVO theory to account for the particle shape [9,14]. Expressions of VDW and EDL for non-spherical particles exist in literature [39–43]. Short expressions can be based on the DA at preferential orientations and distances considering only cylinder radius, and complex expressions can based on the linearized Poisson-Boltzmann equation, Lifshitz equation, Helmholtz equation or others. For those reasons, investigating the effects of shape and orientation of a cylinder interacting with a surface using those approaches can be geometrically limited and mathematically extensive and complex. The DLVO theory has been modified using surface element integration (SEI) to account not only for the shape but also for the particle orientation relative to a surface [14]. Moreover, the SEI resolves limitations in the DA. Therefore, the SEI method is suitable for investigating the effects of shape, orientation, and aspect ratio on particle interaction with a surface.

Cylinders, which geometrically represent carbon nanotubes or certain microorganisms, may have broad aspect ratios, ranging from very high ones in case of carbon nanotubes to very low ones in the case of bacteria. Typical dimensions of carbon nanotubes [11–13,15] are $400 - 5000$ nm length and $0.8 - 30$ nm diameter, aspect ratio of $80 - 1000$. Typical dimensions of bacteria [44–46] are $400 - 8000$ nm length and $300 - 1500$ nm diameter, aspect ratio of $1 - 10$. Furthermore, cylinders can be hollow in the case of a CNT or solid in the case of a bacteria. The SEI approach has previously been applied to investigate the interaction of hollow cylinders of high aspect ratio with surfaces for various orientation angle [14]. However, the effect of the aspect ratio and orientation on the interaction of solid and hollow cylindrical particles have not yet been systematically investigated until now. Furthermore, the effect of the aspect ratio of particles has been experimentally investigated in self-assembly, biomedical, retention and transport applications even though it has not been studied inside the DLVO framework, experimentally or theoretically. Therefore, in this study, we theoretically investigate the manner in which the DLVO interaction energies behave depending on the aspect ratio and orientation of solid and hollow cylinders by applying the SEI method. The cylinders in this study have the properties of a SWCNT because this material is relevant in nanoparticle manufacturing and environmental studies.

2. Numerical methods

A schematic of the interaction of a cylinder particle with a flat surface can be observed in Fig. 1. The SEI approach [9,14] was used to calculate the total interaction energy for a cylindrical particle with a flat surface for different particle aspect ratios and surface orientations using the geometry shown in Fig. 1 and the following governing equation: [9,14]

$$U(D, \varphi, S_i) = \int_{S_i} \hat{n}_i \bullet \hat{k}\, E(h_i)\, dS_i \tag{1}$$

where $U(D,\varphi, S_i)$ is the total interaction energy of surface S_i on a cylindrical particle with a flat surface, the subscript $i = 1, 2, 3$ on parameters denote the top, side, and bottom surfaces of the cylinder, respectively, D is the distance from the center of the cylinder to the flat surface, φ is the orientation angle that the long axis of the particle makes with the surface normal, $\hat{n}_i$ is the outer unit vector normal to the cylinder surface element dS_i, $\hat{k}$ is a unit vector normal to the flat surface, and $E(h_i)$ is the unit interaction energy between the surface element and the flat surface at a local distance of h_i. The value of h_i is the distance between the surface element and the flat surface.

The differential area of the surface element dS_i of a solid cylinder is given as follows: [14]

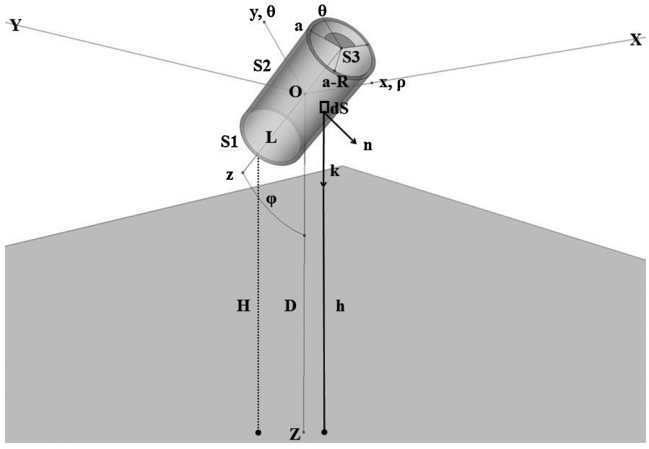

Fig. 1. Schematic of the interaction of a hollow cylinder with a flat surface. The body-fixed (xyz) and space-fixed (XYZ) coordinates originate at center O. The body-fixed coordinates are rotated at an interaction angle (φ) relative to XYZ. A detailed description of all the symbols and their mathematical expressions is provided in the materials and methods section.

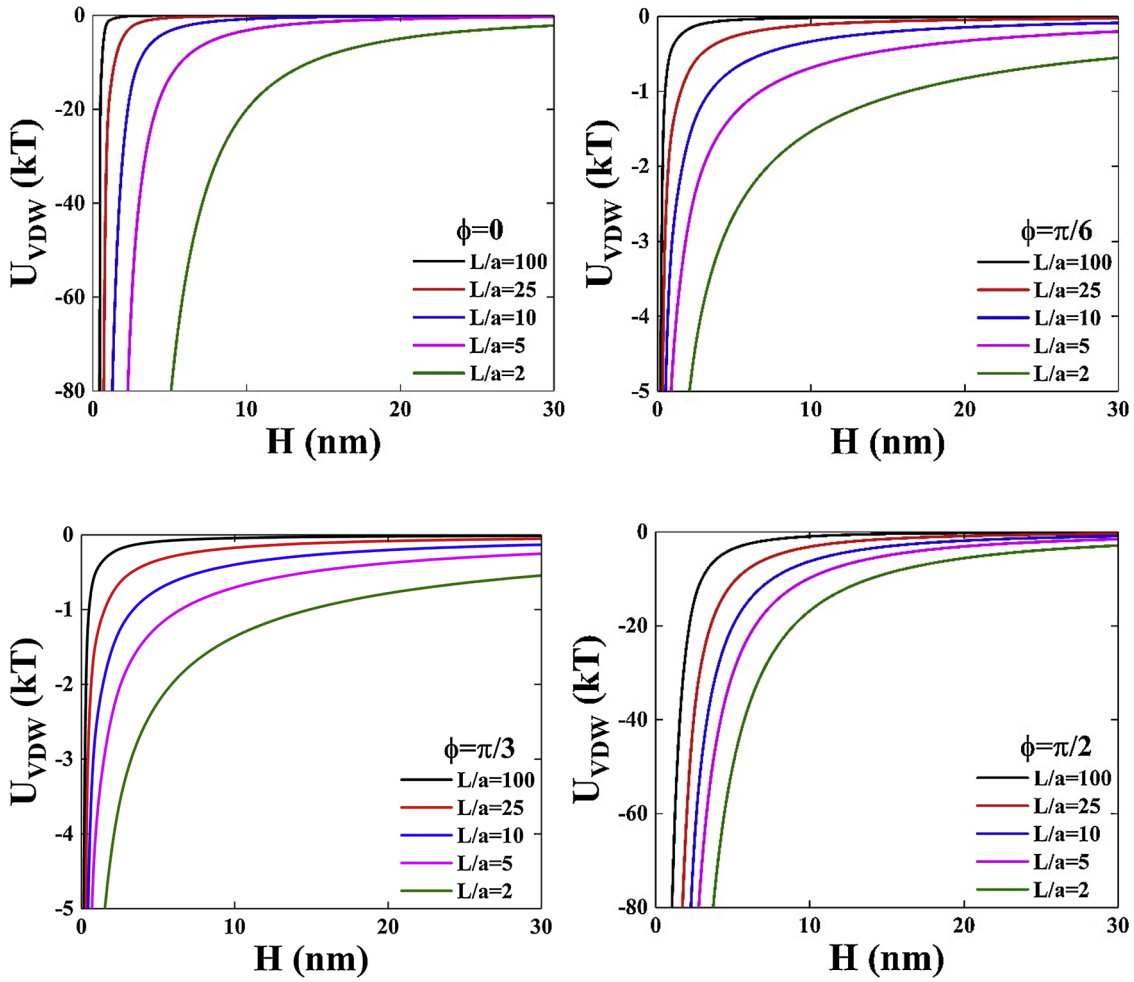

Fig. 2. van der Waals interaction energy between a solid cylinder and a flat surface at an ionic strength of 0.1 M. The energy predictions with the closest separation distance and interaction angle according to the aspect ratio. The aspect ratio is given by the semi-axis L divided by the radius a. Note the difference of scale in the Y-axis.

$$dS_1 = \rho d\rho\, d\theta$$
$$dS_2 = a dz\, d\theta$$
$$dS_3 = \rho d\rho\, d\theta \quad (2)$$

where a is the semi-axis of the cylindrical particle along the x and y axes, ρ and θ are the radial and azimuthal coordinates in a cylindrical coordinate system, respectively. The quantities, $\hat{n}_i$, $\hat{k}$, and h_i can be determined as follows: [14]

$$\hat{n}_1 \bullet \hat{k} = \cos\varphi$$
$$\hat{n}_2 \bullet \hat{k} = \sin\theta\sin\varphi$$
$$\hat{n}_3 \bullet \hat{k} = -\cos\varphi \quad (3)$$

$$h_1 = D - L\cos\varphi - \rho\sin\varphi\sin\theta$$
$$h_2 = D - z\cos\varphi - a\sin\varphi\sin\theta$$
$$h_3 = D + L\cos\varphi - \rho\sin\varphi\sin\theta \quad (4)$$

where $D = H + L\cos\varphi + a\sin\varphi$, H is the distance of minimum approach, and L is the semi-axis of a cylinder directed along the z axis.

The total DLVO interaction energy for each surface element with the flat surface is the sum of VDW and EDL interactions as follows:

$$E(h_i) = E_{VDW}(h_i) + E_{EDL}(h_i) \quad (5)$$

The VDW is a body interaction and EDL is a surface interaction [47–49]. Expressions for the VDW and EDL interactions were obtained from the Hamaker approach [47] and the linear superposition expression [48], respectively, as:

$$E_{VDW}(h_i) = -\frac{A}{12\pi {h_i}^2} \quad (6)$$

$$E_{EDL}(h_{S_i}) = 32\varepsilon_0\varepsilon_1\gamma_c\gamma_s\left(\frac{kT}{ve}\right)^2 \exp(-\kappa h_i) \quad (7)$$

where A is the Hamaker constant for the cylinder–water–surface system (the surface was quartz and the cylinder had the properties of a SWCNT because it is a particle of environmental relevance as mentioned in the introduction), ε_0 is the permittivity of vacuum, ε_1 is the relative permittivity of the solution, γ is the Boltzman factor of the work required to bring an ion from infinity to a location where the charge is ψ as $\gamma = \tanh(ve\psi/4\,kT)$ for a cylinder (denoted with subscript c) or a flat surface (denoted with subscript s), v is the valence of the electrolyte, e is the electron charge, k is the Boltzmann constant, T is the temperature, ψ is the surface charge taken as the zeta potential, and κ is the Debye–-Huckel inverse length of the ion layer.

The total interaction energy of a solid cylinder, $U(D,\varphi)$, is simply given as:

$$U(D, \varphi) = U(D, \varphi, S_1) + U(D, \varphi, S_2) + U(D, \varphi, S_3) \quad (8)$$

In contrast, the value of $U(D,\varphi)$ is more complicated for a hollow cylindrical particle that is water filled. In this case, the inner, water filled, cylinder surface (S_{2IN}) also needs to be considered in the calculation. The separation distance and differential area of this surface element is given as [14]

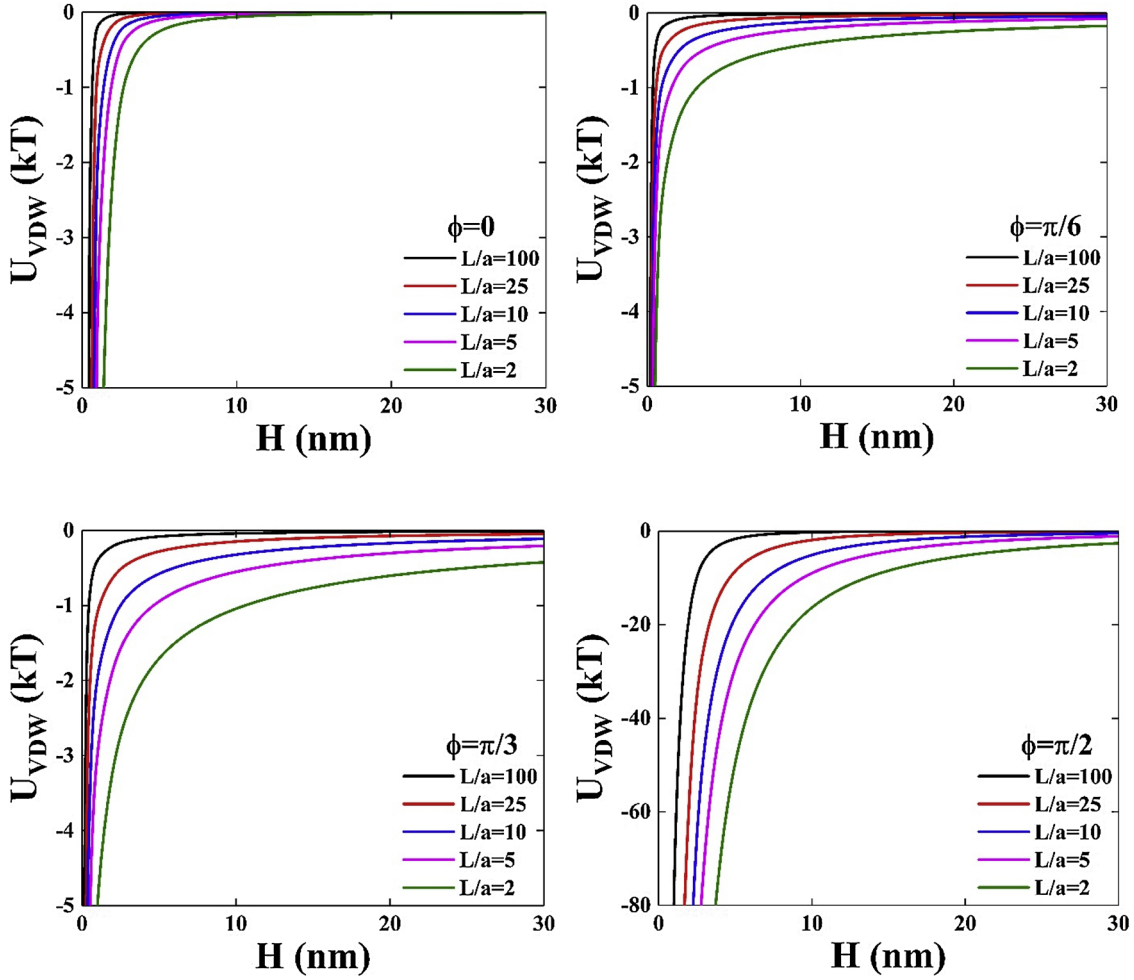

Fig. 3. van der Waals interaction energy between a hollow cylinder and a flat surface at an ionic strength of 0.1 M. The energy predictions are with the closest separation distance and interaction angle according to the aspect ratio. The aspect ratio is given by the semi-axis *L* divided by the radius *a*. Note the difference of scale in the Y-axis.

$$dS_{2IN} = (a - R)\, dz d\theta$$
$$h_{2IN} = \mathrm{D} - \mathrm{zcos}\varphi - (a - R)\mathrm{sin}\varphi\mathrm{sin}\theta \quad (9)$$

where R is the thickness of the cylindrical particle along the smaller axis. An additional surface integration of the van der Waals interaction (U_{VDW}) over S_{2IN} needs to be conducted similar to Eqs. (1–6). The value of $U(D,\varphi)$ for a hollow, water filled, cylindrical particle is then given as: [14,50]

$$U(D, \varphi) = U(D, \varphi, S_1) + U(D, \varphi, S_2) + U(D, \varphi, S_3) - U_{VDW}(D, \varphi, S_{2IN}) \quad (10)$$

Here the lower limit of integration on ρ for surfaces S_1 and S_3 are equal to 0 and a-R for solid and hollow cylindrical particles, respectively. In addition, a hollow cylinder has open ends, and thus the S_{2IN} may contribute to the EDL interaction. However, the exposed part of S_{2IN} is relatively small according to the orientation. Therefore, we have assumed that its contribution to the EDL interaction is negligible.

The above approach was used to calculate the DLVO interactions for hollow and solid cylinders with aspect ratios from 2 to 1000. The aspect ratio is given by the semi-axis L divided by the radius a of a cylinder. The cylinders were assumed to have the properties of a surface-modified SWCNT, and the calculations were performed at an ionic strength (IS) of 0.1 and 0.001 M of a monovalent salt. Further, the average zeta potentials of the surface-modified SWCNT and the flat surface (silica mineral) were −34.50 and −38.81 mV at high IS (0.1 M) and −44.5 and −52.07 mV at low IS (0.001 M), respectively [14,50–53]. The length of the SWCNT was fixed to 400 nm and the Hamaker constant of the SWCNT–water–surface system was 9.81×10^{-21} J [14] at 298.15 K.

3. Results and discussion

The VDW interaction between a solid cylinder and a flat surface is presented in Fig. 2 as a function of H for various aspect ratios (L/a) and orientations with the surface (φ). A decrease in H produces an increase in the VDW attraction as predicted by Eq. (6) (proportional to $1/h_i^2$). For a given φ the strength of the VDW interaction energy increases over a larger range in H as the aspect ratio decreases. This occurs because more particle surface area interacts with the flat surface when a increases and the aspect ratio decreases. The figure also shows that the strength of the VDW interaction is dependent on φ. Specifically, the strength of the VDW interaction increases with φ in the following order, $0 \approx < \pi/6 \approx < \pi/3 < \pi/2$ rad for aspect ratios ≥10 and $\pi/6 \approx < \pi/3 < < 0 < \pi/2$ rad for aspect ratios < 10. This trend has not previously been reported in the literature. This dependence of VDW on φ is predicted by Eqs. (3) and (4) due to differences in the interacting surfaces, h_i, and $\hat{n}_i \bullet \hat{k}$. Surface S_2 exclusively contributes to the interaction energy when $\varphi = \pi/2$ rad, and this produces the largest VDW attraction because it has a greater interacting surface area and smallest separation distances for the considered aspect ratios. In contrast, only surfaces S_1 and S_3 contribute to the interaction energy when $\varphi = 0$ rad. This produces a very weak VDW interaction when the aspect ratio is high (low

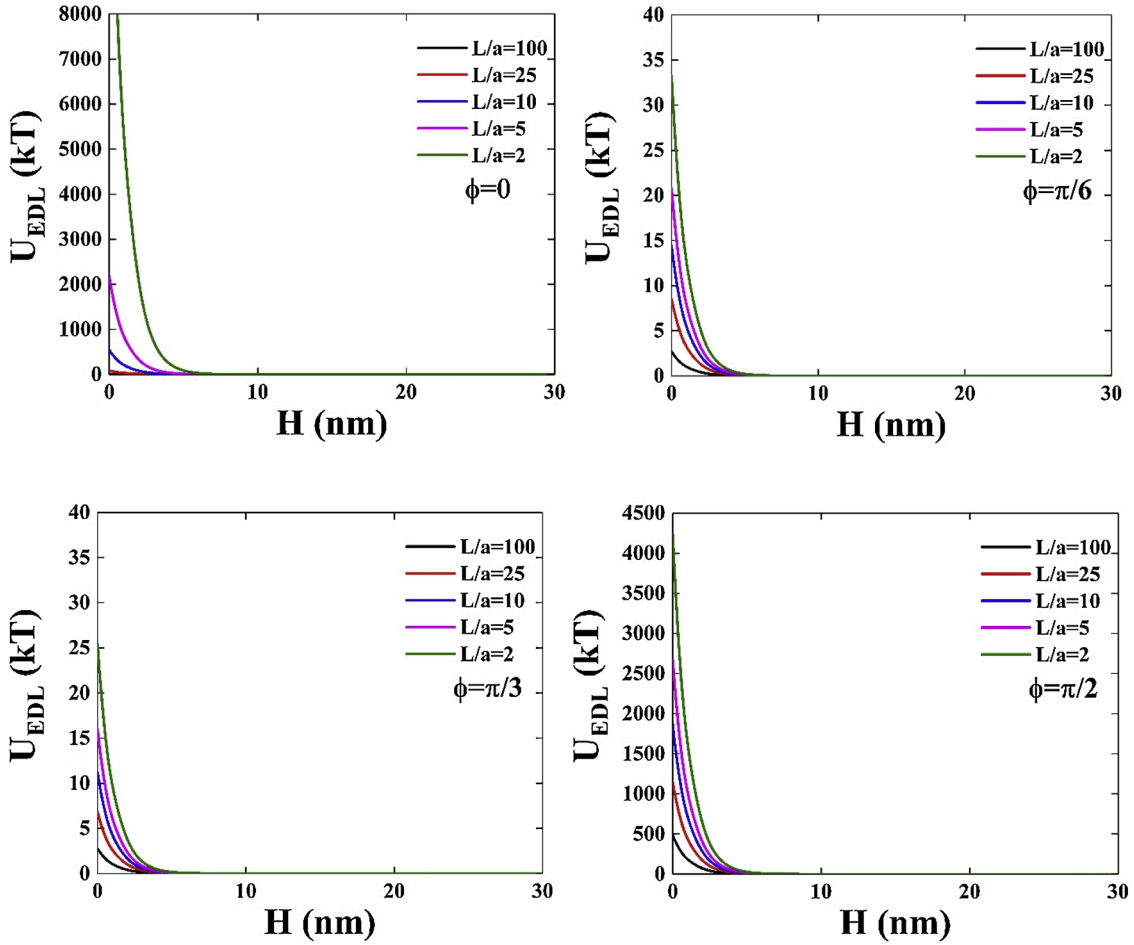

Fig. 4. The electrostatic double layer interaction energy between a solid cylinder and a flat surface at an ionic strength of 0.1 M. The energy predictions are with the closest separation distance and interaction angle according to the aspect ratio. The aspect ratio is given by the semi-axis L divided by the radius a. Note the difference of scale in the Y-axis.

interacting area) but becomes stronger for smaller aspect ratios (higher interacting area). All three surfaces influence interaction energy calculations when $0 < \varphi < \pi/2$ rad. In this case, an increase in φ decreases the relative contribution of S_1 and increases that of S_2. The strength of the VDW interaction increases with φ when the aspect ratio is ≥ 10 because the maximum value of h_2 is smaller and this increases the contribution of the domain surface S_2. A different dependency on φ occurs when the aspect ratio is < 10 because surface S_1 tends to domain the interaction.

The VDW interaction between a hollow cylinder and a flat surface is presented in Fig. 3 as a function of H for various aspect ratios (L/a) and orientations with the surface (φ) when $R = 0.154$ nm (one diameter of carbon atom in the case of a SWCNT). Results in Fig. 3 generally follow the same trends as Fig. 2 for H, the aspect ratio, and φ. However, comparison of Figs. 2 and 3 reveals that the VDW attraction was reduced for the hollow cylinder in comparison to the solid cylinder. Eq. (10) indicates that this is because the VDW attraction is equal to that of the outer solid cylinder minus that for inner cylinder defined by surface S_{2IN}. When $\varphi = \pi/2$ rad the VDW interaction is only reduced on S_2. In addition, the lower limit of integration on ρ for surfaces S_1 and S_3 are equal to 0 and a-R for solid and hollow cylindrical particles, respectively. This exclusively reduces the VDW contribution on surfaces S_1 and S_3 when $\varphi = 0$, π/6, and π/3 rad. Note that this reduction in the VDW interaction was much more pronounced when $\varphi = 0$ rad than when $\varphi = \pi/2$ rad because the value of R was very small (0.154 nm). All surfaces contribute to the interaction when $0 < \varphi < \pi/2$ rad; with S_1 dominating for lower (< 10) aspect ratios and lower φ, and S_2 controlling for higher (≥ 10) aspect ratios and higher φ. Consequently, the reduction in the VDW interaction was greater for lower aspect ratio and for lower φ. Overall, the strength of the VDW attraction increased with φ as $0 < \pi/3 < \pi/6 < \pi/2$ rad for all investigated aspect ratios. Similarly, the strength of the VDW interaction has been reported to increase as the aspect ratio decreased for hollow SWCNT with aspect ratios of 1000 and 133 at one φ, and to increase with φ when the aspect ratio equaled 285 [14]. In this work, it is shown that these same trends apply for a wider range of aspect ratios and φ.

The EDL interaction between a solid cylinder and a flat surface can be observed in Fig. 4 as a function of H for various aspect ratios (L/a) and orientations with the surface (φ). A decrease in H produces an exponential increase in the repulsive EDL interaction as predicted by Eq. (7). For a given φ the strength of the EDL interaction increases as the aspect ratio decreases when $H < 5$ nm. This occurs because more particle surface area is available to interact with the surface when a increases and the aspect ratio decreases. The figure also shows that the strength of the repulsive EDL interaction is dependent on φ. Specifically, the strength of the repulsive EDL interaction increases with φ in the following order: $0 < \pi/3 < \pi/6 < < \pi/2$ rad for L/a of 100, $\pi/3 < \pi/6 < < 0 < < \pi/2$ rad for $5 \leq L/a < 100$, and $\pi/3 < \pi/6 < < \pi/2 < < 0$ rad for L/a of 2. These trends have not been previously reported in the literature and are predicted by Eqs. (3) and (4). Similar to VDW interactions, this dependency of EDL interaction on the aspect ratio and φ is due to differences in the relative contributions of S_1 and S_2. The strength of the EDL interaction increases with φ when the aspect ratio is ≥ 10 because the maximum value of h_2 is smaller and

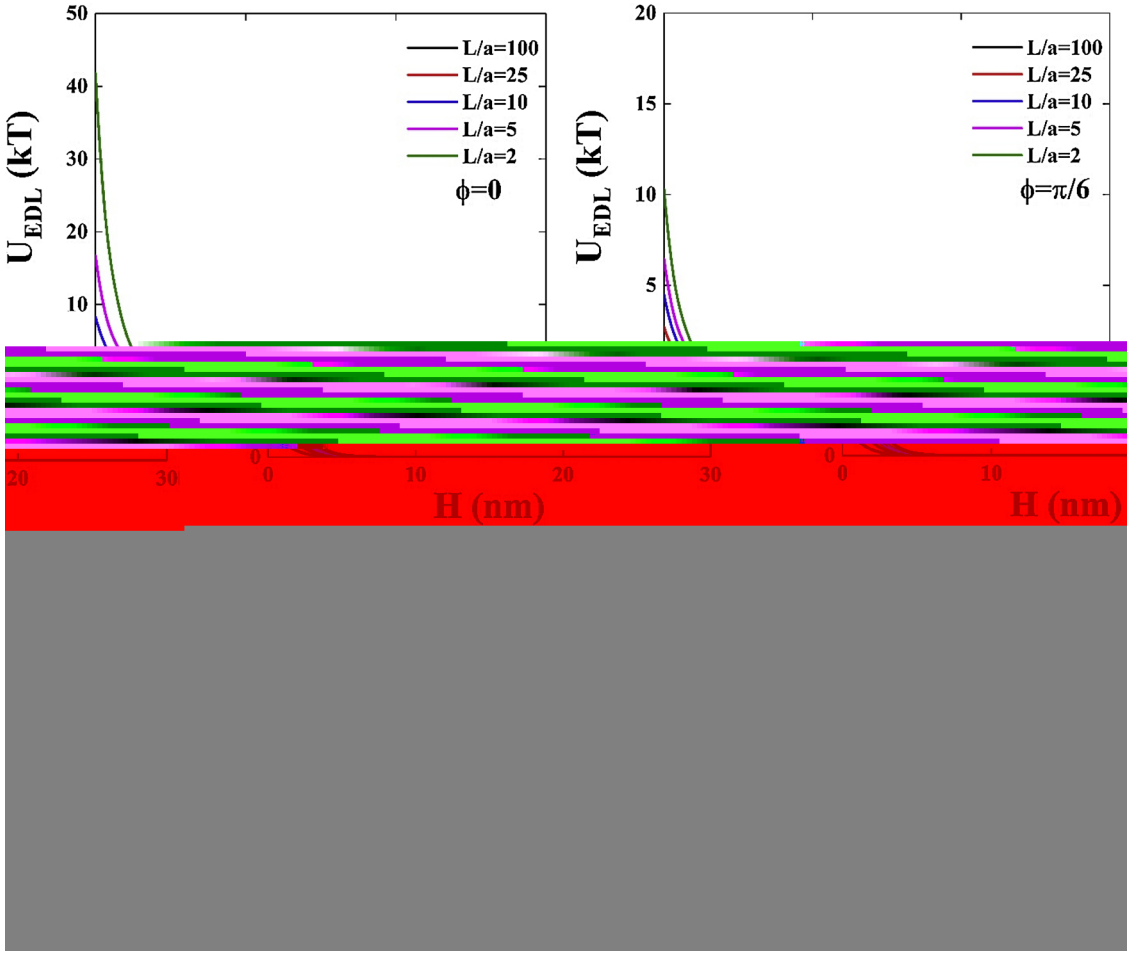

Fig. 5. The electrostatic double layer interaction energy between a hollow cylinder and a flat surface at an ionic strength of 0.1 M. The energy predictions are with the closest separation distance and interaction angle according to the aspect ratio. The aspect ratio is given by the semi-axis *L* divided by the radius *a*. Note the difference of scale in the Y-axis.

this increases the contribution of the domain surface S_2. A different dependency on φ occurs when the aspect ratio is < 10 because surface S_1 tends to control the interaction. As seen in Eq. (7), the exponential term increases as the product of $-\kappa \cdot h_i$ decreases producing more repulsion at lower h_i. When the aspect ratio is 2 the EDL repulsion is greater at 0 rad than at π/2 rad because h_1 is smaller than h_2, even though the area is slightly smaller at 0 rad than at π/2 rad.

The EDL interaction between a hollow cylinder and a flat surface is presented in Fig. 5 as a function of H for various aspect ratios (L/a) and orientations with the surface (φ) when $R = 0.154$ nm. Comparison of Figs. 4 and 5 reveal that the EDL repulsion was reduced for the hollow cylinder in comparison to the solid cylinder when $\varphi = 0$ rad. The limits of integration indicate that when $\varphi = 0$ rad the S_1 of the hollow cylinder is actually a ring having a small area. This causes considerably weaker EDL repulsions than the EDL repulsions of a solid cylinder. When $\varphi = \pi/2$ rad the EDL interaction is dictated only by S_2. Eq. (10) indicates that the strength of the EDL interaction is the same for solid and hollow cylinders because the EDL is a surface interaction (e.g., it is not influenced by the hollow interior). Reductions in the EDL for the hollow cylinder when $0 < \varphi < \pi/2$ are therefore only due to the influence of S_1 and S_3. The strength of the repulsive EDL interaction increased with φ in as follows, $0 < \pi/6 < \pi/3 < \ < \pi/2$ rad for aspect ratios ≥100 and $\pi/6 < \pi/3 < 0 < \ < \pi/2$ rad for aspect ratios < 100. It has been previously reported [14] that the strength of the EDL increased with φ as $0 < \pi/6 < \pi/4 < \pi/2$ rad when the aspect ratio was 285.

The summation of the attractive VDW and repulsive EDL interaction energies produces the total DLVO interaction energy profile according to Eq. (5). The DLVO interaction between a solid cylinder and a flat surface is presented in Fig. 6 as a function of H for various aspect ratios (L/a) and orientations with the surface (φ). For all aspect ratios and angles, the attractive VDW is dominant at $H > 4$ nm producing a finite secondary minimum. The VDW controls this minimum, and it becomes deeper as the aspect ratio decreases because the strength of the VDW increases with the aspect ratio. The repulsive EDL is dominant at $1 < H < 4$ nm producing an energy barrier (EB). Values of the EB for solid cylinders of various aspect ratios at different φ are provided in Table 1. The EB height increases with φ as: $0 < \pi/6 < \pi/3 < \ < \pi/2$ rad for aspect ratios ≥200, as $\pi/3 \approx < \pi/6 < 0 < \ < \pi/2$ rad for $67 \leq L/a < 200$, and as $\pi/3 < \pi/6 < \ < 0 < \pi/2$ rad for aspect ratios < 67. There is a shift in the EB height order between 0 and π/2 rad when the aspect ratio is 2 that can be expressed as $\pi/3 < \pi/6 < \ < \pi/2 < \ < 0$ rad. This occurs when $\varphi = 0$ rad because the EDL interaction becomes considerably stronger than when $\varphi = \pi/2$ rad because of a closer approach distance of the surface elements. In this case, the EDL interaction controls the EB. The smallest EB occurs at an angle of π/3 rad because the VDW and EDL interactions are the weakest at this angle and their summation results in small values of EB when the aspect ratio is ≤67. The VDW dominates at $H < 1$ nm producing an "infinite" energy sink.

The DLVO interaction between a hollow cylinder and a flat surface is presented in Fig. 7 as a function of H for various aspect ratios (L/a) and orientations with the surface (φ) when $R = 0.154$ nm. Results in Fig. 7 generally follow the same trend as Fig. 6 for H, the aspect ratio, and φ. However, comparison of Figs. 6 and 7 reveal that the DLVO

Fig. 6. The DLVO profiles of the total interaction energy between a solid cylinder and a flat surface at an ionic strength of 0.1 M. The energy predictions are with the closest separation distance and interaction angle according to the aspect ratio. The aspect ratio is given by the semi-axis *L* divided by the radius *a*. Note the difference of scale in the Y-axis.

Table 1
The interaction energy barriers between a solid, or a hollow, cylinder and a flat surface at an ionic strength of 0.1 M for a monovalent electrolyte according to the aspect ratio. The aspect ratio is given by the semi-axis L divided by the radius a. The interaction energy was calculated as the sum of van der Waals and electrostatic interactions.

L = 200 nm		Energy barrier (kT) of a solid cylinder				$(a\text{-}R^{b})/a$	Energy barrier (kT) of a hollow cylinder			
a (nm)	L/a	φ^{a} = 0	π/6	π/3	π/2		0	π/6	π/3	π/2
0.2	1000	0.011	0.034	0.088	14.0	0.230	0.011	0.033	0.088	15.6
1	200	0.281	0.352	0.486	62.8	0.846	0.080	0.190	0.408	73.4
2	100	1.126	0.910	0.902	109.0	0.923	0.167	0.335	0.700	119.3
3	67	2.532	1.413	1.203	144.5	0.949	0.253	0.444	0.918	153.4
8	25	18.0	2.830	2.041	257.3	0.981	0.687	0.795	1.561	262.2
20	10	112.6	4.317	3.065	415.5	0.992	1.727	1.241	2.366	417.7
40	5	450.2	5.773	4.136	592.1	0.996	3.460	1.695	3.213	593.3
100	2	2813.9	8.492	6.209	941.8	0.998	8.660	2.558	4.854	942.3

[a] The angle of interaction is in radians.
[b] R is a constant value of 0.152 nm.

interaction was reduced for the hollow cylinder in comparison to the solid cylinder, especially when $\varphi = 0$ rad. In addition, the values of the EBs for various aspect ratios at different φ are provided in Table 1. The EB values increases with φ in the following order, $0 < \pi/6 < \pi/3 < < \pi/2$ rad for aspect ratios ≥ 25. This trend was also found in previous literature [14] for aspect ratios of 1000, 500, 285, 200, and 67. Nevertheless, the increase in EB height with φ can be expressed as $\pi/6 < 0 \approx < \pi/3 < < \pi/2$ rad for aspect ratio $10 \leq L/a < 25$, and $\pi/6 < \pi/3 < 0 < < \pi/2$ rad for $L/a < 10$ because the strength of the EDL interaction becomes weaker at intermediate angles even when L/a decreases to 2 and 5.

Results for the hollow cylinder approach that of the solid cylinder when R is increased (Table 1). The total interaction energy for a hollow cylinder on S_2 increases with an increase in R because it produces a smaller S_{2IN} and therefore less subtraction from the inner cylinder (Eq. 10). Similarly, the lower limit of integration on ρ for surfaces S_1 and S_3 (e.g., a-R) also decrease as R increases and this increases the total interaction energy contribution on S_1. Table 1 indicates that the total

On the other hand, the EBs at π/3 and π/2 rad are slightly bigger for a hollow cylinder than for a solid cylinder. This is because the VDW attraction of a hollow cylinder is just slightly weaker than that of a solid cylinder when $\varphi = \pi/3$ and π/2 rad. The S_2 has a greater contribution than S_1 at these angles. The subtracted interior of a hollow cylinder does not greatly influence the VDW attraction (body interaction) producing slightly smaller VDW interactions than a solid cylinder. The EDL repulsion (surface interaction) is practically the same because the exterior S_2 mostly provides the EDL interactions, thus the EB of a hollow cylinder is slightly smaller than the EB of a solid cylinder. Fig. 9 presents the EB of solid and hollow cylinders as a function of aspect ratio for various φ. The figure demonstrates the angular dependence of the EB according to the aspect ratio. Intermediate angles of π/3 and π/6 rad give the lowest EB for solid and hollow cylinders. For a given low aspect ratio, a solid cylinder shows minimum EBs at π/3 rad while a hollow cylinder shows minimum EBs at π/6 rad.

The EBs for solid and hollow cylinders of various aspect ratios at different φ at an IS of 0.001 M are provided in Table 2. Note that the VDW interaction does not depend on the IS. On the contrary, the exponential decay of the EDL interaction distance strongly depends on the Debye–Huckel inverse length which is defined by the solution chemistry. A high IS compresses the double layer thickness that reduces the EB and may increase the depth of secondary energy minimum. Conversely, a decrease in the IS increases the EB and the secondary minimum can practically disappear. Table 2 shows that the EBs of a hollow cylinder are smaller than of a solid cylinder, and that the EB increases as the aspect ratio decreases. Additionally, Fig. 10 shows a comparison of the EB between a solid and a hollow cylinder for different aspect ratios and φ at an IS of 0.001 M. In the case of a hollow cylinder for all aspect ratios inside the range of 2–1000, the EB increases from a minimum value at 0 rad to a maximum value at π/2 rad. On the other hand in the case of a solid cylinder for aspect ratios inside the range of 25–1000, the EB increases from a minimum value at 0 rad to a maximum value at π/2 rad. Outside this range, the EB increases as $\pi/3 \approx < \pi/6 < 0 < < \pi/2$ for an aspect ratio of $10 \leq L/a < 25$ and as $\pi/3 < \pi/6 < 0 < \pi/2$ for aspect ratios < 10. Compared to the EBs at a higher IS (Fig. 8), the range of monotonic increase is wider for both hollow (2–1000) and solid (25–1000) cylinders. This is because the EDL interaction becomes more dominant at low IS decreasing the EB especially at low φ ($0 \leq \varphi \leq \pi/6$ rad).

An important remark is that this work applies to nanoparticles and bacteria because the aspect ratio can be the same for both particle dimensions. For example, a nanoparticle of length of 100 nm and diameter of 50 nm and a bacteria of length of 1 μm and diameter of 0.5 μm will have the same aspect ratio of 2. The difference will be in the magnitudes of the VDW, EDL and total DLVO interaction energies, where the nanoparticle will yield smaller magnitudes than those of the bacteria but the trends will be the same with the ones presented in this work. This is demonstrated in Table 3 that presents the EB of a micro scale cylinder of length of 4000 nm (size comparable to bacteria; see the introduction) and different diameters. The cylinder has properties of a bacteria with charge of −3.73 mV interacting with a quartz surface of charge −66.7 mV in a IS of 0.0001 M KCl, and the Hamaker constant of the bacteria-quartz-water system is 6.5×10^{-21} J [54].

Fig. 9. The interaction energy barriers between solid and hollow cylinders and a flat surface at an ionic strength of 0.1 M according to angle of interaction as a function of aspect ratio. The interaction energy was calculated as the sum of van der Waals and electrostatic interactions. The angle represents the orientation angle that the long axis of the cylinder makes with the surface normal. The y axis is in log scale.

4. Conclusions

This study examined the interaction energy as a function of distance for solid and hollow cylindrical particles with a flat surface for different particle aspect ratios and surface orientations. Surfaces S_1 and S_3 exclusively contribute to particle interactions when $\varphi = 0$ rad, whereas S_2 only influences interactions when $\varphi = \pi/2$ rad. Surfaces S_1, S_2 and S_3 influence the interaction energies when $0 < \varphi < \pi/2$ rad. In this case, an increase in φ and aspect ratio decreases and increases the relative contributions of S_1 or S_3 and S_2, respectively, due to differences in the interacting surface area and the distance of the surface elements with the flat surface. The VDW interaction of a hollow cylinder is determined by subtracting the VDW interactions of a solid outer and hollow inner cylinders. Consequently, the VDW interaction of a solid cylinder are considerably stronger and operates over longer separation distances than those of a hollow cylinder. The EDL interaction of both solid and hollow cylinders operate at short distances. Furthermore, the strength of the EDL interaction of a solid cylinder is similar to that of a hollow cylinder, especially when $\varphi = \pi/2$ rad and except when $\varphi = 0$ rad where

Table 2
The interaction energy barriers between a solid, or a hollow, cylinder and a flat surface at an ionic strength of 0.001 M for a monovalent electrolyte according to the aspect ratio. The aspect ratio is given by the semi-axis L divided by the radius a. The interaction energy was calculated as the sum of van der Waals and electrostatic interactions.

L = 200 nm		Energy barrier (kT) of a solid cylinder				Energy barrier (kT) of a hollow cylinder			
a (nm)	L/a	φ[a] = 0	π/6	π/3	π/2	0	π/6	π/3	π/2
0.2	1000	0.006	0.128	0.382	7.145	0.005	0.128	0.382	7.371
1	200	0.140	0.717	1.953	35.5	0.040	0.656	1.911	39.1
2	100	0.562	1.676	4.010	70.2	0.083	1.317	3.785	75.2
3	67	1.264	2.878	6.131	104.0	0.126	1.970	5.606	109.7
8	25	8.968	11.4	17.0	263.6	0.343	5.043	14.0	267.6
20	10	56.2	37.5	39.2	559.9	0.862	11.3	30.0	561.9
40	5	224.7	74.5	64.5	897.3	1.727	19.4	48.5	898.5
100	2	1404.1	140.1	110.4	1522.9	4.321	35.3	83.0	1523.4

[a] The angle of interaction is in radians.

Declaration of Competing Interest

The authors declare that they have no known competing financial interests or personal relationships that could have appeared to influence the work reported in this paper.

Acknowledgements

This research was supported by the Basic Science Research Program through the National Research Foundation of Korea (NRF) funded by the Ministry of Education (NRF-2015R1D1A3A01020766) and the selection of research-oriented professor of Chonbuk National University in 2019.

References

[1] S.J. Blott, K. Pye, Particle shape: a review and new methods of characterization and classification, Sedimentology 55 (1) (2008) 31–63.
[2] N. Chatterjee, M. Flury, Effect of particle shape on capillary forces acting on particles at the air-water interface, Langmuir 29 (25) (2013) 7903–7911.
[3] T. Knappenberger, S. Aramrak, M. Flury, Transport of barrel and spherical shaped colloids in unsaturated porous media, J. Contam. Hydrol. 180 (2015) 69–79.
[4] J.Y. Shang, M. Flury, Y.J. Deng, Force measurements between particles and the air-water interface: implications for particle mobilization in unsaturated porous media, Water Resour. Res. 45 (2009).
[5] K. Li, H.L. Ma, Deposition dynamics of rod-shaped colloids during transport in porous media under favorable conditions, Langmuir 34 (9) (2018) 2967–2980.
[6] Z. Adamczyk, P. Weronski, Application of the DLVO theory for particle deposition problems, Adv. Colloid Interface Sci. 83 (1–3) (1999) 137–226.
[7] A. Kuijk, A. van Blaaderen, A. Imhof, Synthesis of monodisperse, rodlike silica colloids with tunable aspect ratio, J. Am. Chem. Soc. 133 (8) (2011) 2346–2349.
[8] M. Hermansson, The DLVO theory in microbial adhesion, Colloids Surf. B Biointerfaces 14 (1–4) (1999) 105–119.
[9] S. Bhattacharjee, J.Y. Chen, M. Elimelech, DLVO interaction energy between spheroidal particles and a fiat surface, Colloids Surf. A Physicochem. Eng. Asp. 165 (1–3) (2000) 143–156.
[10] M. Wang, B. Gao, D.S. Tang, Review of key factors controlling engineered nanoparticle transport in porous media, J. Hazard. Mater. 318 (2016) 233–246.
[11] N.B. Saleh, L.D. Pfefferle, M. Elimelech, Aggregation kinetics of multiwalled carbon nanotubes in aquatic systems: measurements and environmental implications, Environ. Sci. Technol. 42 (21) (2008) 7963–7969.
[12] E. Heister, C. Lamprecht, V. Neves, C. Tilmaciu, L. Datas, E. Flahaut, B. Soula, P. Hinterdorfer, H.M. Coley, S.R.P. Silva, J. McFadden, Higher dispersion efficacy of functionalized carbon nanotubes in chemical and biological environments, ACS Nano 4 (5) (2010) 2615–2626.
[13] Y.A. Tian, B. Gao, C. Silvera-Batista, K.J. Ziegler, Transport of engineered nanoparticles in saturated porous media, J. Nanopart. Res. 12 (7) (2010) 2371–2380.
[14] L. Wu, B. Gao, Y. Tian, R. Munoz-Carpena, K.J. Zigler, DLVO interactions of carbon nanotubes with isotropic planar surfaces, Langmuir 29 (12) (2013) 3976–3988.
[15] A. Mekonen, P. Sharma, F. Fagerlund, Transport and mobilization of multiwall carbon nanotubes in quartz sand under varying saturation, Environ. Earth Sci. 71 (8) (2014) 3751–3760.
[16] C.J. Shih, S.C. Lin, M.S. Strano, D. Blankschtein, Understanding the stabilization of single-walled carbon nanotubes and graphene in ionic surfactant aqueous solutions: large-scale coarse-grained molecular dynamics simulation-assisted DLVO theory, J Phys Chem C 119 (2) (2015) 1047–1060.
[17] S.L. Eichmann, B. Smith, G. Meric, D.H. Fairbrother, M.A. Bevan, Imaging carbon nanotube interactions, diffusion, and stability in nanopores, ACS Nano 5 (7) (2011) 5909–5919.
[18] J.S. McNown, J. Malaika, Effects of particle shape on settling velocity at low Reynolds numbers, Eos Trans. AGU 31 (1) (1950) 74–82.
[19] P. Belouschek, D. Lorenz, Z. Adamczyk, Calculation of electrostatic interaction forces between ellipsoidal particles, Colloid Polym. Sci. 269 (5) (1991) 528–531.
[20] S.C. Glotzer, M.J. Solomon, N.A. Kotov, Self-assembly: from nanoscale to microscale colloids, AIChE J. 50 (12) (2004) 2978–2985.
[21] D. Chapot, L. Bocquet, E. Trizac, Electrostatic potential around charged finite rodlike macromolecules: nonlinear Poisson-Boltzmann theory, J. Colloid Interf. Sci. 285 (2) (2005) 609–618.
[22] S. Sacanna, L. Rossi, B.W.M. Kuipers, A.P. Philipse, Fluorescent monodisperse silica ellipsoids for optical rotational diffusion studies, Langmuir 22 (4) (2006) 1822–1827.
[23] M.B. Salerno, M. Flamm, B.E. Logan, D. Velegol, Transport of rodlike colloids through packed beds, Environ. Sci. Technol. 40 (20) (2006) 6336–6340.
[24] S. Badaire, C. Cottin-Bizonne, J.W. Woody, A. Yang, A.D. Stroock, Shape selectivity in the assembly of lithographically designed colloidal particles, J. Am. Chem. Soc. 129 (1) (2007) 40–41.
[25] J.N. Dong, D.S. Corti, E.I. Franses, Y. Zhao, H.T. Ng, E. Hanson, Colloidal dispersion stability of CuPc aqueous dispersions and comparisons to predictions of the DLVO theory for spheres and parallel face-to-Face cubes, Langmuir 26 (10) (2010) 6995–7006.
[26] D.R. Heine, M.K. Petersen, G.S. Grest, Effect of particle shape and charge on bulk rheology of nanoparticle suspensions, J. Chem. Phys. 132 (18) (2010).
[27] S. Aramrak, M. Flury, J.B. Harsh, R.L. Zollars, H.P. Davis, Does colloid shape affect detachment of colloids by a moving air-water interface? Langmuir 29 (19) (2013) 5770–5780.
[28] V. Malik, B. Grobety, V. Trappe, H. Dietsch, P. Schurtenberger, A closer look at the synthesis and formation mechanism of hematite nanocubes, Colloids Surf. A Physicochem. Eng. Asp. 445 (2014) 21–29.
[29] R. Toy, P.M. Peiris, K.B. Ghaghada, E. Karathanasis, Shaping cancer nanomedicine: the effect of particle shape on the in vivo journey of nanoparticles, Nanomedicine-Uk 9 (1) (2014) 121–134.
[30] V.R. Dugyala, M.G. Basavaraj, Evaporation of sessile drops containing colloidal rods: coffee-ring and order-disorder transition, J. Phys. Chem. B 119 (9) (2015) 3860–3867.
[31] P.M.P. Lins, V.S. Marangoni, T.M. Uehara, P.B. Miranda, V. Zucolotto, J. Cancino-Bernardi, Differences in the aspect ratio of gold nanorods that induce defects in cell membrane models, Langmuir 33 (50) (2017) 14286–14294.
[32] D. Nepal, M.S. Onses, K. Park, M. Jespersen, C.J. Thode, P.F. Nealey, R.A. Vaia, Control over Position, orientation, and spacing of arrays of gold nanorods ssing chemically nanopatterned surfaces and tailored particle-particle-surface interactions, ACS Nano 6 (6) (2012) 5693–5701.
[33] H. Herd, N. Daum, A.T. Jones, H. Huwer, H. Ghandehari, C.M. Lehr, Nanoparticle geometry and surface orientation influence mode of cellular uptake, ACS Nano 7 (3) (2013) 1961–1973.
[34] H. Meng, S. Yang, Z.X. Li, T. Xia, J. Chen, Z.X. Ji, H.Y. Zhang, X. Wang, S.J. Lin, C. Huang, Z.H. Zhou, J.I. Zink, A.E. Nel, Aspect ratio determines the quantity of mesoporous silica nanoparticle uptake by a small GTPase-Dependent macropinocytosis mechanism, ACS Nano 5 (6) (2011) 4434–4447.
[35] Y.F. Zhao, G. Cavallaro, Y. Lvov, Orientation of charged clay nanotubes in evaporating droplet meniscus, J. Colloid Interf. Sci. 440 (2015) 68–77.
[36] B.Y. Lv, L.S. Zhao, Y. Pu, Y. Le, X.F. Zeng, J.F. Chen, N. Wen, J.X. Wang, Facile preparation of controllable-aspect-Ratio hydroxyapatite nanorods with high-gravity technology for bone tissue engineering, Ind. Eng. Chem. Res. 56 (11) (2017) 2976–2983.
[37] G.A. Rance, D.H. Marsh, S.J. Bourne, T.J. Reade, A.N. Khlobystov, Van der waals interactions between nanotubes and nanoparticles for controlled assembly of composite nanostructures, ACS Nano 4 (8) (2010) 4920–4928.
[38] C. Shen, Y. Jin, J. Zhuang, T. Li, B. Xing, Role and importance of surface heterogeneities in transport of particles in saturated porous media, Crit. Rev. Environ. Sci. Technol. (2019) 1–86.
[39] D.W. Langbein, Theory of Van Der Waals Attraction, Springer Tracts in Modern Physics, Springer-Verlag, Berlin; New York, 1974, pp. 1–139 145 pages.
[40] L.R. White, On the deryaguin approximation for the interaction of macrobodies, J. Colloid Interf. Sci. 95 (1) (1983) 286–288.
[41] H. Ohshima, Electrostatic interaction between two parallel cylinders, Colloid Polym. Sci. 274 (12) (1996) 1176–1182.
[42] H. Ohshima, Electrostatic interaction between a cylinder and a planar surface, Colloid Polym. Sci. 277 (6) (1999) 563–569.
[43] J.N. Israelachvili, Intermolecular and Surface Forces, 3rd ed., Academic Press, Burlington, 2011 Mass..
[44] T.H. Weiss, A.L. Mills, G.M. Hornberger, J.S. Herman, Effect of bacterial cell shape on transport of bacteria in porous media, Environ. Sci. Technol. 29 (7) (1995) 1737–1740.
[45] W.P. Van De Merwe, J. Czege, M.E. Milham, B.V. Bronk, Rapid optically based measurements of diameter and length for spherical or rod-shaped bacteria in vivo, Pure Appl. Opt. J. Eur. Opt. Soc. Part A 43 (28) (2004) 5295–5302.
[46] G. Kim, K. Park, J. Choi, A. Gomez-Flores, Y. Han, S.Q. Choi, H. Kim, Bioflotation of malachite using different growth phases of *Rhodococcus opacus*: effect of bacterial shape on detachment by shear flow, Int. J. Miner. Process. 143 (2015) 98–104.
[47] H.C. Hamaker, The London—van der Waals attraction between spherical particles, Physica 4 (10) (1937) 1058–1072.
[48] J. Gregory, Interaction of unequal double-layers at constant charge, J. Colloid Interf. Sci. 51 (1) (1975) 44–51.
[49] C.Y. Shen, S. Bradford, Z. Wang, Y.F. Huang, Y.L. Zhang, B.G. Li, DLVO interaction energies between hollow spherical particles and collector surfaces, Langmuir 33 (40) (2017) 10455–10467.
[50] C.Y. Shen, S.A. Bradford, M. Flury, Y.F. Huang, Z. Wang, B.G. Li, DLVO interaction energies for hollow particles: the filling matters, Langmuir 34 (43) (2018) 12764–12775.
[51] P. Wang, Q.H. Shi, H.J. Liang, D.W. Steuerman, G.D. Stucky, A.A. Keller, Enhanced environmental mobility of carbon nanotubes in the presence of humic acid and their removal from aqueous solution, Small 4 (12) (2008) 2166–2170.
[52] H.C. Li, P.L. Debruyn, Electrokinetic and adsorption studies on quartz, Surf. Sci. 5 (2) (1966) 203-&..
[53] H.N. Kim, S.A. Bradford, S.L. Walker, *Escherichia coli* O157:H7 transport in saturated porous media: role of solution chemistry and surface macromolecules, Environ. Sci. Technol. 43 (12) (2009) 4340–4347.
[54] H.N. Kim, S.L. Walker, S.A. Bradford, Macromolecule mediated transport and retention of *Escherichia coli* O157:H7 in saturated porous media, Water Res. 44 (4) (2010) 1082–1093.